Eikonal Equation Reproduces Natural Landscapes With Threshold Hillslopes

AGU ADVANCING EARTH AND SPACE SCIENCES

Geophysical Research Letters®

RESEARCH LETTER
10.1029/2023GL105710

Eikonal Equation Reproduces Natural Landscapes With Threshold Hillslopes

Shashank Kumar Anand[1], Matteo B. Bertagni[1,2], Arvind Singh[3], and Amilcare Porporato[1,2]

[1]Department of Civil and Environmental Engineering, Princeton University, Princeton, NJ, USA, [2]High Meadows Environmental Institute, Princeton University, Princeton, NJ, USA, [3]Department of Civil, Environmental and Construction Engineering, University of Central Florida, Orlando, FL, USA

Key Points:

- The simple eikonal model describes the landscape morphology with threshold hillslopes
- The natural landscape's slope-area relation establishes the boundary condition for the model
- The model results faithfully reproduce diverse landforms, such as islands, an inland volcano, and a mountain range

Supporting Information:

Supporting Information may be found in the online version of this article.

Correspondence to:

S. K. Anand,
skanand@princeton.edu

Citation:

Anand, S. K., Bertagni, M. B., Singh, A., & Porporato, A. (2023). Eikonal equation reproduces natural landscapes with threshold hillslopes. *Geophysical Research Letters*, *50*, e2023GL105710. https://doi.org/10.1029/2023GL105710

Received 31 JUL 2023
Accepted 16 OCT 2023

Author Contributions:

Conceptualization: Shashank Kumar Anand, Matteo B. Bertagni, Amilcare Porporato
Funding acquisition: Amilcare Porporato
Investigation: Shashank Kumar Anand
Methodology: Shashank Kumar Anand
Software: Shashank Kumar Anand
Supervision: Arvind Singh, Amilcare Porporato
Validation: Shashank Kumar Anand
Visualization: Shashank Kumar Anand
Writing – original draft: Shashank Kumar Anand
Writing – review & editing: Matteo B. Bertagni, Arvind Singh, Amilcare Porporato

Abstract Many natural landscapes maintain steep planar hillslopes bounded at a typical angle, beyond which shallow landslides or slope failures remove the excess sediment volume by mass wasting. Here we show that the celebrated eikonal equation, derived from a landscape evolution model in conditions of negligible soil diffusion and fluvial erosion, accurately portrays the organization of these topographies. Referred to as "eikonal landscapes," such solutions feature constant-slope hillslopes originating from downstream boundary conditions and culminating in sharp upstream ridges. We demonstrate that the eikonal landscapes reproduce well a variety of natural landforms, including small islands, a volcano, and an extended mountain ridge. The boundary condition for the eikonal representation is specified through the natural landscape's slope-area relation. Going beyond merely representing landscape statistical features, the present results provide a first-of-kind direct match of mathematical and natural landscapes.

Plain Language Summary Natural terrains often feature steep and nearly flat hillslopes, which remain stable up to a threshold angle or the angle of repose. Beyond this angle, mass failure ensues, resulting in the removal of excess sediment volume and preserving the topography. Here we demonstrate the effective use of the eikonal model, originally developed to represent the propagation of light rays two centuries back, in describing the organization of threshold hillslopes in natural landscapes. We directly compare eikonal model-generated topographies with various natural landscapes, including islands, volcanoes, and inland mountains, differing in size, underlying geology, and climatic conditions. The presented model achieves these results with minimal computational cost compared to traditional landscape evolution simulations.

1. Introduction

Observations of almost planar hillslopes in many steep landscapes (Figure 1) suggest that these hillslopes remain stable up to a threshold value (Binnie et al., 2007; Carson & Petley, 1970; Korup, 2008; Montgomery, 2001; Ouimet et al., 2009; Penck, 1953; Stock & Dietrich, 2003; Strahler, 1950; Whipple et al., 1999). Such threshold-hillslope terrains attain a dynamic equilibrium, where any further steepening of hillslopes removes excess sediment by mass wasting failure, leaving the topography unchanged. This geomorphological setting is analogous to the table-top experiment of building a pile by adding granular material over a table, where the topography is bounded by the threshold angle at which cohesion and friction forces balance gravity (Al-Hashemi & Al-Amoudi, 2018; Nadai, 1954; Pauli & Gioia, 2007). In natural landscapes, the threshold angle, or the angle of repose, is determined by various interrelated factors, including the type of rock or soil characteristics (Korup, 2008; Montgomery & Brandon, 2002; Strahler, 1950), climate conditions (Gabet et al., 2004), surface and sub-surface flow properties (G. E. Tucker & Slingerland, 1994; Montgomery & Dietrich, 1994).

Both climate and geology determine the presence of threshold-hillslope terrains, which are commonly found in regions that have experienced recent episodes of mountain building, such as the young mountain ranges of the Tibetan plateau (Blöthe et al., 2015; Burbank et al., 1996; Hodges, 2000; Larsen & Montgomery, 2012; Ouimet et al., 2009), as opposed to older undulating hills of the Appalachian range (Hibbard, 2000). Over geological timescales, fluvial erosion gradually wears down uplifted topography below the angle of repose, leading to the formation of concave valleys (G. E. Tucker & Bras, 1998; Fernandes & Dietrich, 1997; Rodriguez-Iturbe & Rinaldo, 2001; Bonetti & Porporato, 2017; Seybold et al., 2021). In environments conducive to glacial and fluvial erosion, igneous rocks, which are less susceptible to surface erosion, exhibit greater resilience in maintaining threshold hillslopes when compared to weaker sedimentary rocks (Zondervan et al., 2020). Stratovolcanoes

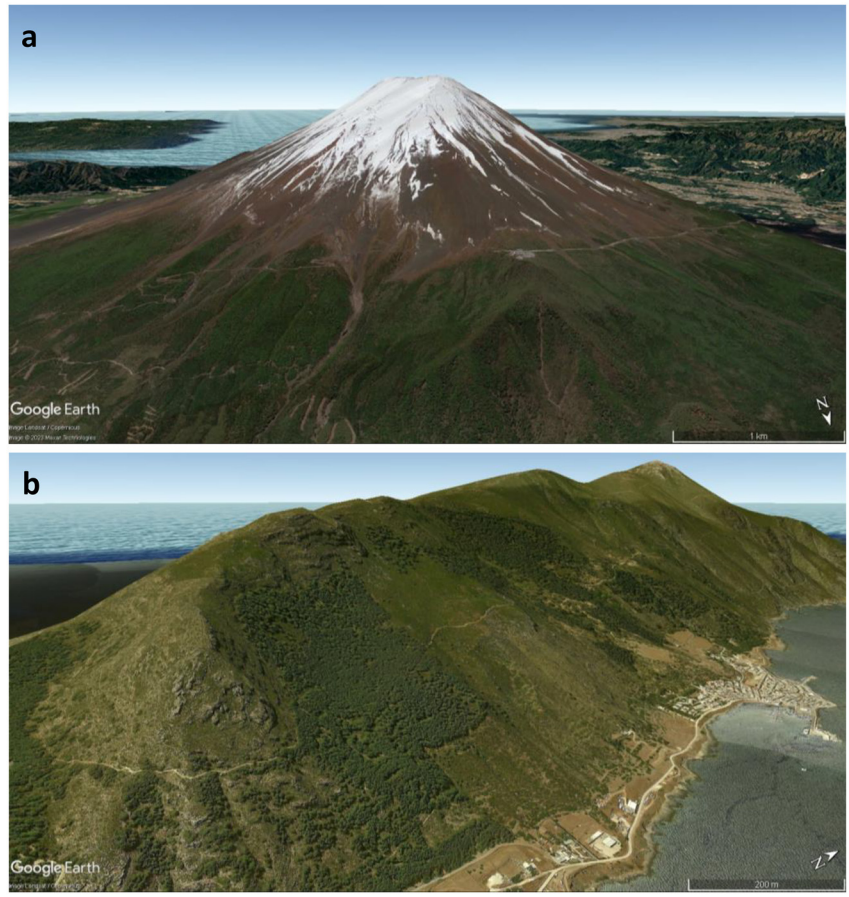

Figure 1. Example of landscapes with threshold hillslopes. (a) Conically shaped Mount Fuji (35°21′42″N, 138°43′39″E) in Japan, with a summit height of around 3,700 m. (b) Marettimo Island (37°58′15″N, 12°03′25″E) in the Egadi Archipelago, Italy, with a summit height of around 700 m. Data Source: Google Earth.

are prime examples of threshold-hillslope terrains characterized by nearly symmetrical hillslopes surrounding a crater. These hillslopes are bound by a consistent threshold angle over a range of spatial scales until a high contributing area facilitates sediment erosion through surface runoff (Oguchi & Oguchi, 2010).

Numerous mathematical models have been developed to simulate the intricate dynamics of mass wasting processes. Some have primarily focused on assessing slope stability and predicting landslide occurrences within landscapes (Claessens et al., 2007; Montgomery & Dietrich, 1994). Other models have delved into studying the propagation of debris fronts by utilizing granular and fluid mechanics to examine slope failure events (Ghilardi et al., 2001; Hutter et al., 1994; Iverson & George, 2014). Furthermore, numerical models have been developed to explore topographic evolution under diverse conditions, including the incorporation of stochastic forcing or threshold angles to analyze denudation rates and landscape-scale responses to tectonic or hydroclimatic influences (Hergarten & Neugebauer, 1998; G. E. Tucker & Bras, 1998; Roering et al., 1999; Campforts et al., 2017). While these studies have significantly contributed to our understanding of different slope failure-induced landslide erosion features, the dynamic equilibrium problem of the threshold-hillslope organization remains open.

This study demonstrates that the eikonal equation, previously used for small-scale table top experiments (Al-Hashemi & Al-Amoudi, 2018; Nadai, 1954; Pauli & Gioia, 2007), can accurately simulate the organization of large-scale natural landscapes featuring threshold hillslopes. We derive the eikonal equation (refer to Appendix A for details) as a minimal form of a widely used landscape evolution model (Anand, Bonetti, Camporeale, & Porporato, 2022; Bonetti et al., 2020; Braun & Willett, 2013; Howard, 1994; Izumi & Parker, 1995; Perron et al., 2009), by decoupling sediment and water dynamics, that is, no fluvial erosion, along with the negligible soil diffusion. As a result, the equation and the boundary condition read

$$|\nabla z| = \Theta, \tag{1}$$

$$z(x, y) = z_b \quad \text{at} \quad (x, y) \in \mathcal{B}, \tag{2}$$

where Θ is the threshold angle at the verge of failure for the landscape elevation $z(x, y)$ bounded by the downstream boundary $\mathcal{B}$ at elevation z_b. Conceptually, the threshold angle Θ employed here differs from the critical gradient S_c used in non-linear diffusion models for hillslope processes (Andrews & Bucknam, 1987; Roering et al., 1999), as S_c cannot be observed in the field due to the infinite sediment flux when the surface slope approaches S_c.

Our findings demonstrate that the generated "eikonal landscapes" accurately replicate various natural terrains, ranging from small mountainous islands to a stratovolcano and an extensive mountain range. This is the first direct comparison between model-generated topographies featuring threshold hillslopes and real-world landscapes, encompassing diverse characteristics such as size, underlying geologic setting, and prevailing hydroclimatic condition.

2. Eikonal Landscapes

To evaluate the predictions of the threshold hillslope organization based on eikonal landscapes, we examine their applicability in four distinct natural terrains across the globe. Our case studies encompass two Mediterranean islands and two inland mountain regions: (a) Marettimo Island in the west of Sicily, Italy, covering an area of approximately 15 km^2; (b) Gyaros Island situated in the southeast of the mainland Greece, spanning around 21 km^2; (c) a region encompassing about 35 km^2 around the primary crater of Mount Fuji, Japan's highest stratovolcanic peak; and (d) an expansive Zanskar Mountain Range of approximately 122 km^2 within the Ladakh plateau of India, positioned in the rain shadow of the Great Himalayan range. We utilized ASTER DEM Version 3 (Abrams et al., 2020; Spacesystems & Team, 2019) to obtain elevation data for these case studies.

2.1. Islands

We begin the analysis by considering the topography of Marettimo, a small island characterized by an average slope of approximately 29°. The boundary $\mathcal{B}$ of the eikonal model is defined by the mean sea level, represented as $z_b = 0$ m (Figure 2a). To compare the actual topography of Marettimo Island with the eikonal model solution, we solve Equation 1 using the prescribed boundary condition and $\Theta = 29°$. As depicted in Figure 2c, the obtained eikonal topography captures the primary ridge line and the overall organization of near-planar hillslopes on Marettimo Island.

While the mean sea level serves as the downstream boundary for the island of Marettimo, determining the spatial extent to which slope failure is the primary landscape-formation mechanism is essential for the accurate eikonal reconstruction of other islands and inland mountain ranges. By plotting the average topographic slope against the specific contributing area, we were able to resolve the spatial scales up to which slope failure triggers debris flow (Booth et al., 2013; Brardinoni & Hassan, 2006; Montgomery & Foufoula-Georgiou, 1993; Roering et al., 2007; Singh et al., 2015; Stock & Dietrich, 2003). This analysis enabled us to distinguish between landscapes predominantly shaped by threshold hillslopes and extract the contour boundary $\mathcal{B}$ for eikonal reconstruction (see Figures S1 and S2 and the discussion in Supporting Information S1).

We extend our analysis to include Gyaros Island, an uninhabited landmass spanning approximately 21 km^2, characterized by an arid environment and covered uniformly with numerous shrubs (Vardinoyannis et al., 2015). The slope-area analysis for the island (see Figure S1b in Supporting Information S1) reveals the presence of two dominant regimes of sediment transport, namely a debris-dominated regime at small spatial scales and the fluvial erosion regime at large spatial scales. In Figure 2b, the red contour curve (z_b = 125 m) demarcates the debris-dominated steep topography, which has an average slope of 26°, and the downstream fluvially-lowered topography of the island (Tarboton et al., 1991; G. Tucker & Whipple, 2002; Singh et al., 2015). Additionally, the blue curve signifies the mean sea level in Figures 2b and 2d. By employing the red contour curve as the boundary condition, we construct an eikonal topography that conforms well with the topographic data obtained from the debris-dominated region of Gyaros Island. Figure 2d presents the elevation field ranging from 125 to 484 m in the actual terrain, while the reproduced eikonal topography extends from 125 to 527 m. To validate these

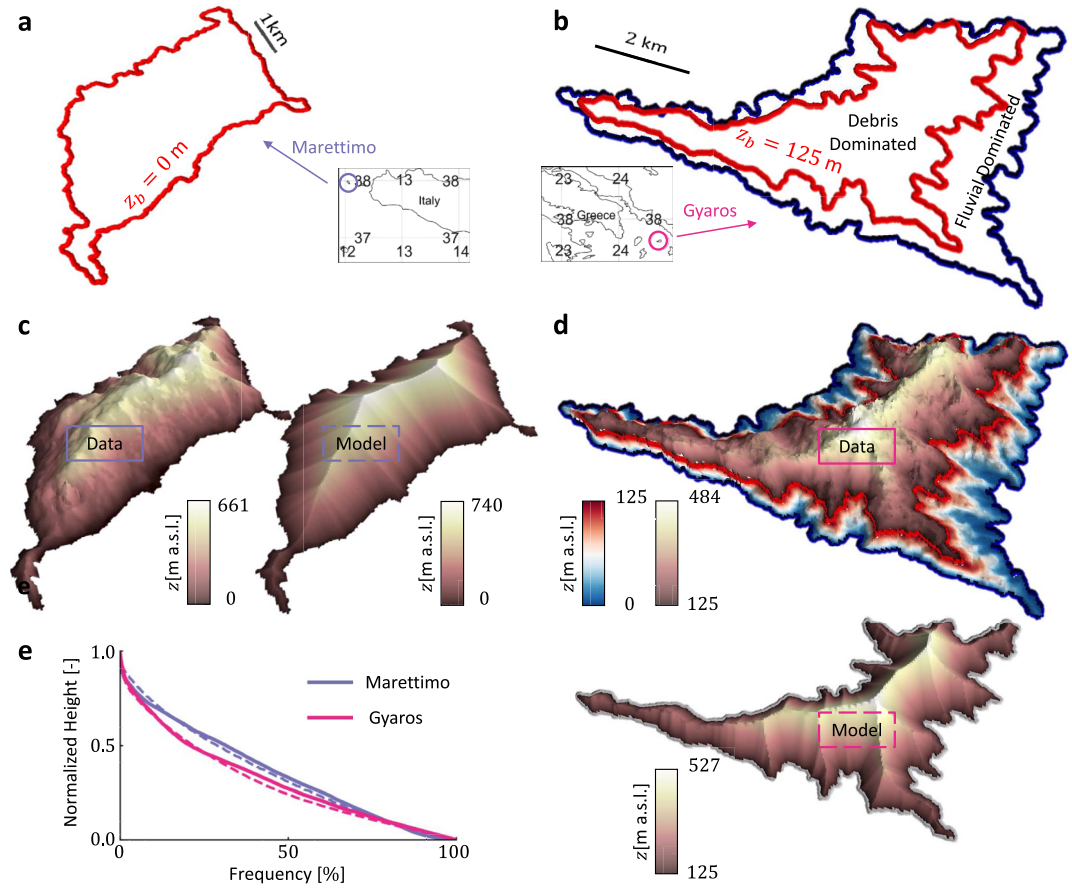

Figure 2. Eikonal landscapes reproduce two Mediterranean islands, namely (a, c) Marettimo and (b,d) Gyaros. (a, b) The red curves are the downstream boundary conditions employed in the eikonal reconstruction for Marettimo Island ($z_b = 0$ m a.s.l.) and Gyaros Island ($z_b = 125$ m a.s.l.). Gyaros Island's (red) boundary separates the upstream debris-dominated landscape from the downstream fluvial regime, ending at sea level (blue curve). The boxes show the islands' geographic locations. (c, d) Comparison between natural and eikonal landscapes for (c) Marettimo Island and (d) Gyaros Island. (e) Hypsometric curves for both the landscape data (solid) and the model topographies (dashed).

visual observations for both Marettimo and Gyaros, we compare the hypsometric plots of the normalized height (Keylock et al., 2020; Ohmori, 1993; Strahler, 1952) derived from the data with the model-generated counterpart (Figure 2e), demonstrating a good agreement.

2.2. Inland Volcano and Mountain Range

We investigate the suitability of the eikonal model in reproducing nearly planar hillslope configurations in two distinct inland mountain ranges. The first geological case study focuses on Mount Fuji, known for its near-conical shape and basalt-rich composition (Oguchi & Oguchi, 2010). The second case pertains to an arid mountain in the Zanskar range, part of the Tethys Himalaya, located in southern Ladakh, India. This mountain comprises a weakly metamorphosed sedimentary series (Dèzes, 1999). Both landscapes exhibit consistently steep average topographic slopes, measuring 27° for Mount Fuji and 32° for Zanskar Mountain. Similar to the technique employed for Gyaros Island, we establish a contour level at the base of the hillslopes, encompassing landscapes primarily shaped by the debris-flow mechanism in these two geological settings (see Figures S1 and S2 in Supporting Information S1).

Figures 3a and 3b provide compelling visual evidence of a good match between the eikonal model solutions that build landscapes by arranging constant-slope hillslopes and the topographic data for two considered landscapes of Mount Fuji and the Zanskar Mountain. Removing the area of the main crater of Mount Fuji, the eikonal topography also rises close to 3,757 m in a near-conical fashion. Figure 3b shows that the model provides a reasonable

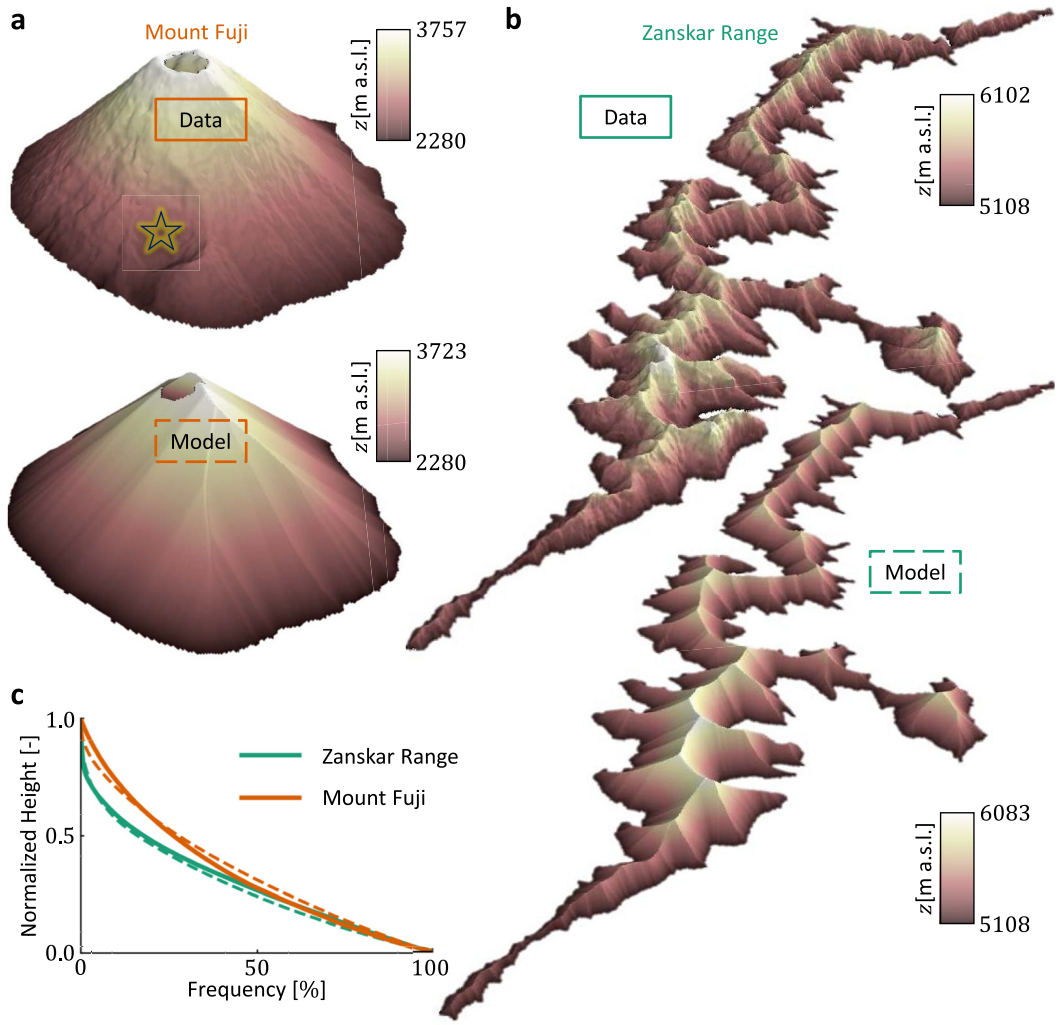

Figure 3. Comparison of natural and eikonal landscapes for (a) Mount Fuji (~35 km^2) in Japan and (b) the arid Zanskar Range (~122 km^2) in the Tethys Himalaya (India). The star symbol in (a) designates the secondary crater formed during the early 18th-century eruption. (c) The hypsometric curves for the landscape data (solid) and the eikonal model solutions (dashed).

spatial arrangement of hillslopes in the Zanskar Range, where the main ridgeline rises up to 6,083 m compared to the digital elevation model (DEM) value of 6,102 m. The visual confirmation of the eikonal model capturing well natural topographies is validated in Figure 3d by comparing the hypsometric curves of the topographic data and model reconstructions.

2.3. Local Defects and Smoothing

As shown in Figures 2 and 3, we have constructed eikonal landscapes for both the island and inland topographies by using a uniform threshold for hillslope stability across the entire landscape and assuming minimal influence of other surface processes at the considered scale of the landscape. While the idealized eikonal topography can be readily updated to account for spatial variations in threshold values based on variable rock strength or subsurface conditions in Equation 1, comparing it to natural topography provides valuable insights into the spatial heterogeneities that exist in real-world landscapes.

Figure 4 presents the polar distribution of the hillslope aspect for the four landscapes under consideration (solid) alongside their corresponding eikonal reconstructions (dashed), with 90° representing the north direction. The results demonstrate good agreement between the aspect distribution of the actual data and the eikonal

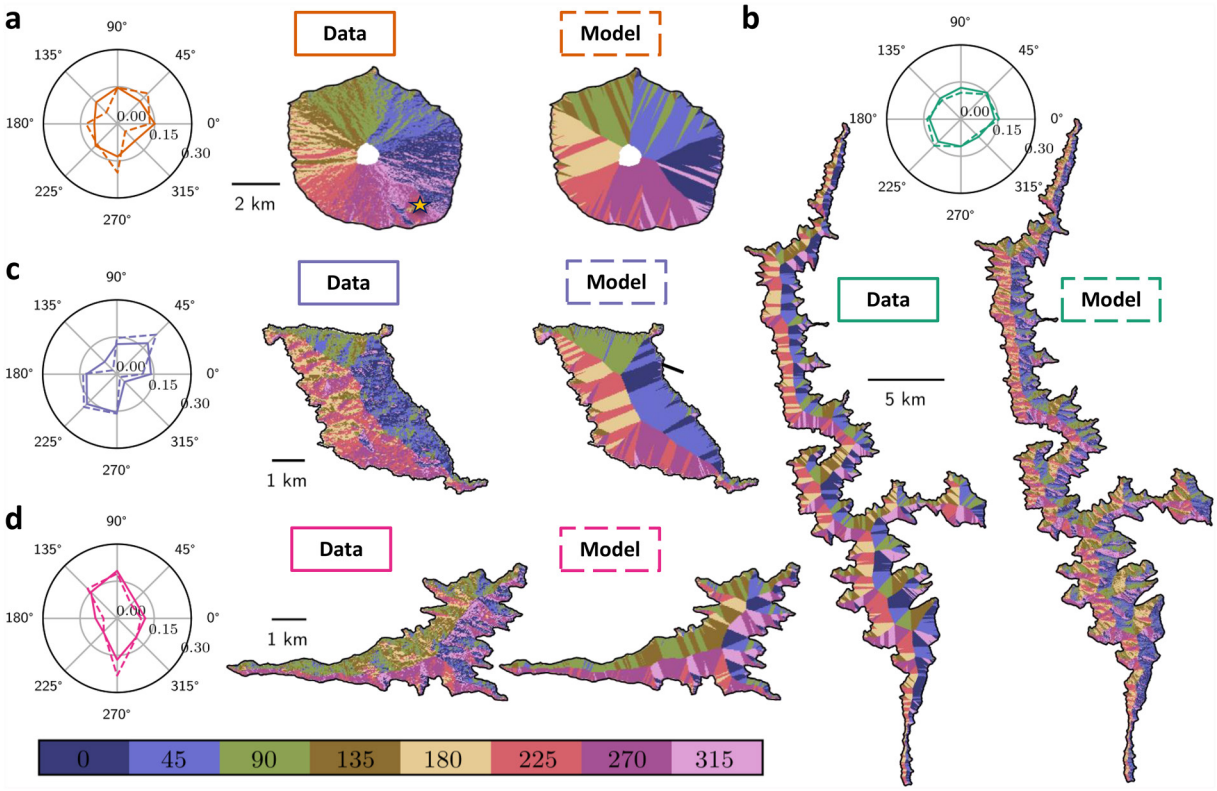

Figure 4. Hillslope aspect distributions for (a) Mount Fuji, (b) Zanskar Mountain, (c) Marettimo Island, and (d) Gyaros Island. Aspect angles are assigned in eight directions from 0° to 315°. Solid/dashed curves indicate the polar histogram for the actual data/the eikonal reconstruction. In each panel, color plots for hillslope aspects are presented with the data on the left and the model reconstructions on the right.

reconstruction across different landscapes. At the same time, some regions can be identified with differences between the model and actual data. To illustrate this, we consider the well-documented case of the secondary crater on Mount Fuji, highlighted in Figure 3a. This secondary crater was formed during an eruption in the early 18th century (Oguchi & Oguchi, 2010), but it is notably absent in the eikonal reconstruction. As a result, the eikonal model overestimates the south-facing slopes, as seen in Figure 4a.

In Figure 5, we compute the difference between actual elevation and eikonal elevation, which we refer to as residual topography, and examine its spatial patterns for both Gyaros Island and Mount Fuji. This analysis of residual topography is similar to the excess topography metric presented by Blöthe et al. (2015). In their work, the authors studied the rock volume above threshold hillslope angles in the Himalaya-Karakoram ranges of Asia. Following the same phrasing, we categorize areas with positive residual topography as excess topography for our model and regions with negative residual as reduced topography. We have identified three primary regions 1, 2,

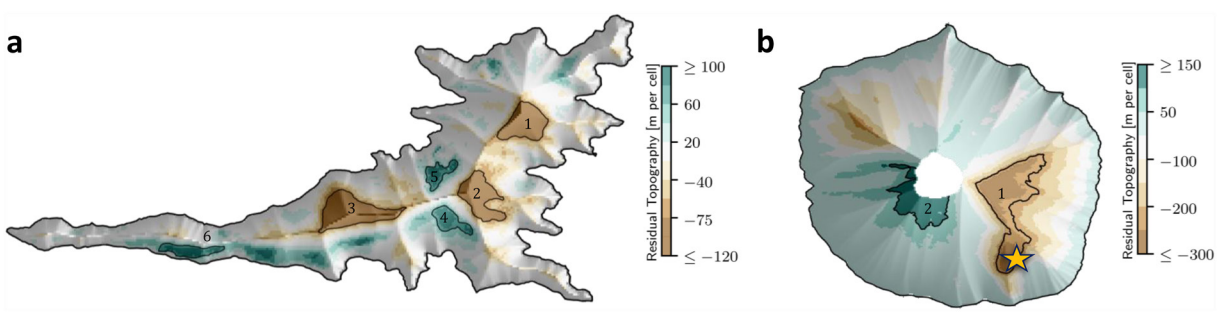

Figure 5. Residual topography for (a) Gyaros Island and (b) Mount Fuji. In (a), regions 1, 2, and 3 highlight areas with reduced topography, while regions 4, 5, and 6 indicate areas with excess topography at $\Theta = 26°$. In (b), regions 1 and 2 represent reduced and excess topography, respectively, at a threshold angle of $\Theta = 27°$.

and 3, where most of the reduced topography exists for Gyaros Island, comprising approximately 7.4% of the total debris-dominated area and a removed volume of around 88 million cubic meters for threshold angle $\Theta = 26°$. Regions 4, 5, and 6, covering around 2.7% of the total area, contain approximately 24 million cubic meters of excess volume for Gyaros Island.

Similarly, we identify regions 1 and 2 as prominent reduced and excess topography areas in Mount Fuji, accounting for 5.1% and 2.6% of the total debris-dominated area around the main crater. Region 1 is at a mean elevation of approximately 2,935 m, situated on the collapsed portion of the hillslope around the secondary crater in the southeast part of Mount Fuji, where the reduced volume is estimated to be around 460 million cubic meters. On the other hand, region 2 is located south of the volcano's main crater at an average height of 3,466 m, containing approximately 116 million cubic meters of excess volume for $\Theta = 27°$. These results show that although the simple eikonal model captures the threshold hillslope organization well on the landscape scale, local departures of the idealized model output from topographic data can be leveraged to uncover spatial heterogeneities in real-world terrains.

Another crucial point to note is the presence of sharp ridges and hilltops in eikonal topographies. In contrast, natural ridges and hilltops present smoother crests and ridges (e.g., Figures 2c and 2d), since soil creep (i.e., diffusion) contributes to smooth the high-frequency components of topographic relief with age (Davis, 1892; Fernandes & Dietrich, 1997; G. E. Tucker & Bras, 1998; Bonetti & Porporato, 2017; Anand & Porporato, 2022). This was also observed in sand-pile experiments (Pauli & Gioia, 2007), implying that, while the eikonal topographies capture the overall configuration of threshold hillslopes, soil diffusion remains crucial for dissipating the sharp ridges and hilltops formed by competing planar hillslopes. This localized diffusion mechanism also occurs on the ridges of fluvial landscapes under intense channelization conditions, where diffusion acts locally to dissipate abrupt changes in the surface slope (Porporato, 2022). Similar localized dissipation mechanisms are responsible for dissipating sharp fronts or shocks in weak solutions of the Euler model and wave propagation (Bec & Khanin, 2007; Kluwick, 2018).

3. Discussion and Conclusions

The eikonal model has a rich history in physics, mathematics, and engineering, including applications in geometric optics (Bruns, 1895), electromagnetism (Masoliver & Ros, 2009; Rukhadze & Silin, 1964), soft matter (Nechaev & Polovnikov, 2017), thin films (Ortiz & Gioia, 1994), mathematical analysis (Achdou et al., 2013; Crandall & Lions, 1983), image processing (Adalsteinsson & Sethian, 1995), robotics (Petres et al., 2007), and semiconductor manufacturing (Sethian & Adalsteinsson, 1997). However, its use in geoscience has been limited, except for applications in seismology (Lambare et al., 2003; Lawton, 1989). In geomorphology, it has been recently employed for modeling coastal depositional morphology reconstruction of debris and alluvial fans (Ke & Capart, 2015; T.-Y. Chen et al., 2022; T.-Y. K. Chen & Capart, 2022).

Similar to the eikonal model, there are several studies using geometric constraints on surface slopes for delta shoreline evolution (Kim & Muto, 2007; Lorenzo-Trueba & Voller, 2010; Lorenzo-Trueba et al., 2012; Swenson et al., 2000). Other variations include using the Hamilton–Jacobi equation (the eikonal equation is a static Hamilton–Jacobi equation) to model fluvial knickpoint propagation (Luke, 1972, 1974; Weissel & Seidl, 1998), the evolution of 1D vertical incision fronts (Aronsson & Linde, 1982) and surface transects along stream profiles (Stark & Stark, 2022). Other than the related concept of excess topography (Blöthe et al., 2015), this work presents a novel application of the eikonal equation to characterize landscapes dominated by threshold hillslopes.

The uniqueness of the eikonal model lies in its simplified form of a nonlinear differential equation, capable of generating distinct constant-slope hillslope configurations based exclusively on the complexity of the domain boundary (Figure S3 in Supporting Information S1). In any mathematical model, describing a system's physics involves both governing equations and boundary conditions (Anand, Bonetti, Camporeale, Hooshyar, & Porporato, 2022; Bursten, 2021). When studying pattern formation, the emphasis is typically placed on governing equations rather than boundary conditions. For example, numerous studies on landscape evolution modeling assume simplified representations of boundary conditions (Anand, Bonetti, Camporeale, & Porporato, 2022; Bonetti et al., 2020; Perron et al., 2009; G. Tucker & Whipple, 2002) to disentangle the complex nonlinear interactions within the governing equations from the external constraints imposed by realistic boundary conditions. Our proposed eikonal approach exemplifies a reversal in the apparent roles of governing equations and boundary

conditions, as it is the information propagated by the intricate downstream boundary that gives rise to various spatial configurations of planar hillslopes.

A major advantage of the eikonal model is its ability to recreate threshold hillslope topography only using the boundary determined on the slope-area relation of natural terrain. This low-input requirement makes the model a powerful tool, especially in situations with limited information or uncertainties in parameter estimations of complex models for the time and space scales relevant to landscape evolution. Additionally, the time complexity of constructing an eikonal landscape exhibits a linear relationship with the number of nodes within the domain, resulting in remarkable efficiency. The computational cost of an eikonal landscape is comparable to a single time-step update of the fluvial erosion term in efficient landscape evolution simulations (Anand et al., 2020; Barnes, 2019; Braun & Willett, 2013). The elevation reconstruction at a specific point relies solely on the shortest distance between that point and the boundary (Pauli & Gioia, 2007), irrespective of its absolute spatial position, showcasing the model's adaptability to any discrete mesh configuration.

Our study demonstrates how the eikonal model accurately reproduces topographies dominated by threshold hillslopes across diverse geological and hydroclimatic settings. This result is particularly notable, considering the inherent heterogeneity and complexity observed at the long timescale of landscape formation. Distinct eikonal reconstructions provide insights into the pivotal role of the downstream boundary in shaping the threshold hillslope arrangement as uplifted landscapes strive for dynamic equilibrium. Irrespective of the downstream boundary complexity, eikonal landscapes consistently depict visibly smooth valleys without extensive branching, aligning with our observations (Figure 1) and previous field-study findings (Stock & Dietrich, 2003). While more elaborate models that incorporate numerous parameters and detailed information on local climate, lithology, and hydrology are valuable for understanding the short-term response of near-planar hillslopes, our findings underscore the relevance of the simple yet effective eikonal model in unraveling the organization of such terrains that have had sufficient time to adapt to prevailing conditions.

Appendix A: Eikonal Model as the Limiting Case of Landscape Evolution Models

The minimalist landscape evolution model is a system of coupled nonlinear partial differential equations for the water and sediment balance (Bonetti et al., 2020). The sediment balance describes the surface elevation dynamics $z(x, y)$ as controlled by uplift, soil creep, and fluvial erosion, which couples the sediment and water dynamics. Here we show that the eikonal equation can be derived as a limiting case of the sediment balance by considering negligible soil creep and decoupling the erosion term from the water continuity equation. At a quasi-steady state, the sediment balance can be written as

$$U + D\nabla^2 z - Ka^m|\nabla z|^n = 0, \tag{A1}$$

where U is the uplift rate, which is modeled as a constant source term; $D\nabla^2 z$ is a linear diffusion term representing soil creep; and $Ka^m|\nabla z|^n$ is detachment-limited fluvial erosion, where m and n are model exponents. a is the specific contributing area that couples the sediment balance to the water balance through the exponent m (Anand, Bonetti, Camporeale, & Porporato, 2022; Bonetti et al., 2020; Royden & Taylor Perron, 2013).

When surface erosion is controlled by landslides and debris flow rather than water runoff, the landscape morphological signature shows an almost constant slope that does not depend on the specific contributing area (regime II of Figure S1a in Supporting Information S1). Namely, the sediment and water equations are decoupled ($m \sim 0$). For negligible soil diffusion, $D \to 0$, Equation A1 reduces to the eikonal equation as

$$|\nabla z| = \Theta, \tag{A2}$$

with $\Theta = (U/K)^{1/n}$ becomes a constant threshold parameter for the model.

Equation A2 provides a solution for arbitrary domain shape, bounded by the downstream boundary $\mathcal{B}$. By solving the first-order differential Equation A2 within a closed boundary, we consider landscape formation under the conditions of vanishing soil diffusion at the landscape scale. Specifically, the effect of soil diffusion becomes localized, dissipating topographic singularities and sharp changes in the surface gradient inside the domain, such as ridges or hilltops that arise from the convergence of competing threshold hillslopes. The vanishing diffusion formulation of the eikonal model shares similarities with surface growth models (Kardar et al., 1986; Qi &

Wang, 2001), fluvial landscape model of evolution (Hooshyar et al., 2020; Porporato, 2022), and the Euler model in fluid dynamics (Bec & Khanin, 2007; Whitham, 2011), where diffusive mechanisms are responsible for dissipating sharp fronts in weak solutions.

Data Availability Statement

The Python code developed for the eikonal simulations is available at Anand (2023).

Acknowledgments
The authors acknowledge support from the Innovation Award - Moore Science-to-Action Fund, the Carbon Mitigation Initiative, and the High Meadows Environmental Institute at Princeton University. We thank the associate editor and reviewers, Vaughan Voller and Wolfgang Schwanghar, for the insightful critique of the manuscript. The numerical analysis in this article was performed on computational resources provided by Princeton Research Computing at Princeton University.

References

Abrams, M., Crippen, R., & Fujisada, H. (2020). Aster global digital elevation model (GDEM) and aster global water body dataset (ASTWBD). *Remote Sensing*, *12*(7), 1156. https://doi.org/10.3390/rs12071156

Achdou, Y., Barles, G., Ishii, H., & Litvinov, G. L. (2013). *Hamilton-Jacobi equations: Approximations, numerical analysis and applications*. Springer Berlin Heidelberg. Retrieved from https://books.google.com/books?id=MiS6BQAAQBAJ

Adalsteinsson, D., & Sethian, J. A. (1995). A fast level set method for propagating interfaces. *Journal of Computational Physics*, *118*(2), 269–277. https://doi.org/10.1006/jcph.1995.1098

Al-Hashemi, H. M. B., & Al-Amoudi, O. S. B. (2018). A review on the angle of repose of granular materials. *Powder Technology*, *330*, 397–417. https://doi.org/10.1016/j.powtec.2018.02.003

Anand, S. K., & Porporato, A. (2022). Increased asymmetry of pit-over-peak statistics with landscape smoothing. *Earth Surface Processes and Landforms*, *47*(1), 298–307. https://doi.org/10.1002/esp.5248

Anand, S. K. (2023). ShashankAnand1996/Eikonal-Model-for-Threshold- Hillslopes: v1.0.0 [Software]. Zenodo. https://doi.org/10.5281/zenodo.8408490

Anand, S. K., Bonetti, S., Camporeale, C., Hooshyar, M., & Porporato, A. (2022). Comment on "groundwater affects the geomorphic and hydrologic properties of coevolved landscapes" by Litwin et al. *Journal of Geophysical Research: Earth Surface*, *127*(10), e2022JF006669. https://doi.org/10.1029/2022JF006669

Anand, S. K., Bonetti, S., Camporeale, C., & Porporato, A. (2022). Inception of regular valley spacing in fluvial landscapes: A linear stability analysis. *Journal of Geophysical Research: Earth Surface*, *127*(11), e2022JF006716. https://doi.org/10.1029/2022JF006716

Anand, S. K., Hooshyar, M., & Porporato, A. (2020). Linear layout of multiple flow-direction networks for landscape-evolution simulations. *Environmental Modelling & Software*, *133*, 104804. https://doi.org/10.1016/j.envsoft.2020.104804

Andrews, D., & Bucknam, R. C. (1987). Fitting degradation of shoreline scarps by a nonlinear diffusion model. *Journal of Geophysical Research*, *92*(B12), 12857–12867. https://doi.org/10.1029/jb092ib12p12857

Aronsson, G., & Linde, K. (1982). Grand Canyon—A quantitative approach to the erosion and weathering of a stratified bedrock. *Earth Surface Processes and Landforms*, *7*(6), 589–599. https://doi.org/10.1002/esp.3290070607

Barnes, R. (2019). Accelerating a fluvial incision and landscape evolution model with parallelism. *Geomorphology*, *330*, 28–39. https://doi.org/10.1016/j.geomorph.2019.01.002

Bec, J., & Khanin, K. (2007). Burgers turbulence. *Physics Reports*, *447*(1–2), 1–66. https://doi.org/10.1016/j.physrep.2007.04.002

Binnie, S. A., Phillips, W. M., Summerfield, M. A., & Fifield, L. K. (2007). Tectonic uplift, threshold hillslopes, and denudation rates in a developing mountain range. *Geology*, *35*(8), 743–746. https://doi.org/10.1130/g23641a.1

Blöthe, J. H., Korup, O., & Schwanghart, W. (2015). Large landslides lie low: Excess topography in the Himalaya-Karakoram ranges. *Geology*, *43*(6), 523–526. https://doi.org/10.1130/g36527.1

Bonetti, S., Hooshyar, M., Camporeale, C., & Porporato, A. (2020). Channelization cascade in landscape evolution. *Proceedings of the National Academy of Sciences of the United States of America*, *117*(3), 1375–1382. https://doi.org/10.1073/pnas.1911817117

Bonetti, S., & Porporato, A. (2017). On the dynamic smoothing of mountains. *Geophysical Research Letters*, *44*(11), 5531–5539. https://doi.org/10.1002/2017GL073095

Booth, A. M., Roering, J. J., & Rempel, A. W. (2013). Topographic signatures and a general transport law for deep-seated landslides in a landscape evolution model. *Journal of Geophysical Research: Earth Surface*, *118*(2), 603–624. https://doi.org/10.1002/jgrf.20051

Brardinoni, F., & Hassan, M. A. (2006). Glacial erosion, evolution of river long profiles, and the organization of process domains in mountain drainage basins of coastal british columbia. *Journal of Geophysical Research*, *111*(F1), F01013. https://doi.org/10.1029/2005jf000358

Braun, J., & Willett, S. D. (2013). A very efficient o(n), implicit and parallel method to solve the stream power equation governing fluvial incision and landscape evolution. *Geomorphology*, *180*, 170–179. https://doi.org/10.1016/j.geomorph.2012.10.008

Bruns, H. (1895). *Das eikonal* (Vol. 21(5)). S. Hirzel

Burbank, D. W., Leland, J., Fielding, E., Anderson, R. S., Brozovic, N., Reid, M. R., & Duncan, C. (1996). Bedrock incision, rock uplift and threshold hillslopes in the northwestern Himalayas. *Nature*, *379*(6565), 505–510. https://doi.org/10.1038/379505a0

Bursten, J. R. (2021). The function of boundary conditions in the physical sciences. *Philosophy of Science*, *88*(2), 234–257. https://doi.org/10.1086/711502

Campforts, B., Schwanghart, W., & Govers, G. (2017). Accurate simulation of transient landscape evolution by eliminating numerical diffusion: The TTLEM 1.0 model. *Earth Surface Dynamics*, *5*(1), 47–66. https://doi.org/10.5194/esurf-5-47-2017

Carson, M. A., & Petley, D. J. (1970). *The existence of threshold hillslopes in the denudation of the landscape* (pp. 71–95). Transactions of the Institute of British Geographers.

Chen, T.-Y., Wu, Y.-C., Hung, C.-Y., Capart, H., & Voller, V. R. (2022). A control volume finite element model for predicting the morphology of cohesive-frictional debris flow deposits. In *Earth surface dynamics discussions* (pp. 1–26).

Chen, T.-Y. K., & Capart, H. (2022). Computational morphology of debris and alluvial fans on irregular terrain using the visibility polygon. *Computers & Geosciences*, *169*, 105228. https://doi.org/10.1016/j.cageo.2022.105228

Claessens, L., Schoorl, J., & Veldkamp, A. (2007). Modelling the location of shallow landslides and their effects on landscape dynamics in large watersheds: An application for northern New Zealand. *Geomorphology*, *87*(1–2), 16–27. https://doi.org/10.1016/j.geomorph.2006.06.039

Crandall, M. G., & Lions, P.-L. (1983). Viscosity solutions of Hamilton-Jacobi equations. *Transactions of the American Mathematical Society*, *277*(1), 1–42. https://doi.org/10.1090/s0002-9947-1983-0690039-8

Davis, W. (1892). The convex profile of bad-land divides. *Science*, *508*, 245. https://doi.org/10.1126/science.ns-20.508.245

Dèzes, P. (1999). *Tectonic and metamorphic evolution of the central Himalayan domain in southeast Zanskar (Kashmir, India) (No. 32)*. Université de Lausanne.
Fernandes, N. F., & Dietrich, W. E. (1997). Hillslope evolution by diffusive processes: The timescale for equilibrium adjustments. *Water Resources Research*, *33*(6), 1307–1318. https://doi.org/10.1029/97wr00534
Gabet, E. J., Pratt-Sitaula, B. A., & Burbank, D. W. (2004). Climatic controls on hillslope angle and relief in the Himalayas. *Geology*, *32*(7), 629–632. https://doi.org/10.1130/g20641.1
Ghilardi, P., Natale, L., & Savi, F. (2001). Modeling debris flow propagation and deposition. *Physics and Chemistry of the Earth - Part C: Solar, Terrestrial & Planetary Science*, *26*(9), 651–656. https://doi.org/10.1016/s1464-1917(01)00063-0
Hergarten, S., & Neugebauer, H. J. (1998). Self-organized criticality in a landslide model. *Geophysical Research Letters*, *25*(6), 801–804. https://doi.org/10.1029/98gl50419
Hibbard, J. (2000). Docking Carolina: Mid-Paleozoic accretion in the southern Appalachians. *Geology*, *28*(2), 127–130. https://doi.org/10.1130/0091-7613(2000)028<0127:dcmpai>2.3.co;2
Hodges, K. V. (2000). Tectonics of the Himalaya and southern Tibet from two perspectives. *Geological Society of America Bulletin*, *112*(3), 324–350. https://doi.org/10.1130/0016-7606(2000)112<324:tothas>2.0.co;2
Hooshyar, M., Anand, S., & Porporato, A. (2020). Variational analysis of landscape elevation and drainage networks. *Proceedings of the Royal Society A*, *476*(2239), 20190775. https://doi.org/10.1098/rspa.2019.0775
Howard, A. D. (1994). A detachment-limited model of drainage basin evolution. *Water Resources Research*, *30*(7), 2261–2285. https://doi.org/10.1029/94wr00757
Hutter, K., Svendsen, B., & Rickenmann, D. (1994). Debris flow modeling: A review. *Continuum Mechanics and Thermodynamics*, *8*(1), 1–35. https://doi.org/10.1007/bf01175749
Iverson, R. M., & George, D. L. (2014). A depth-averaged debris-flow model that includes the effects of evolving dilatancy. I. Physical basis. *Proceedings of the Royal Society A: Mathematical, Physical and Engineering Sciences*, *470*(2170), 20130819. https://doi.org/10.1098/rspa.2013.0819
Izumi, N., & Parker, G. (1995). Inception of channelization and drainage basin formation: Upstream-driven theory. *Journal of Fluid Mechanics*, *283*, 341–363. https://doi.org/10.1017/S0022112095002357
Kardar, M., Parisi, G., & Zhang, Y.-C. (1986). Dynamic scaling of growing interfaces. *Physical Review Letters*, *56*(9), 889–892. https://doi.org/10.1103/physrevlett.56.889
Ke, W.-T., & Capart, H. (2015). Theory for the curvature dependence of delta front progradation. *Geophysical Research Letters*, *42*(24), 10–680. https://doi.org/10.1002/2015gl066455
Keylock, C. J., Singh, A., Passalacqua, P., & Foufoula-Georgiou, E. (2020). Hölder-conditioned hypsometry: A refinement to a classical approach for the characterization of topography. *Water Resources Research*, *56*(5), e2019WR025412. https://doi.org/10.1029/2019wr025412
Kim, W., & Muto, T. (2007). Autogenic response of alluvial-bedrock transition to base-level variation: Experiment and theory. *Journal of Geophysical Research*, *112*(F3), F03S14. https://doi.org/10.1029/2006jf000561
Kluwick, A. (2018). Shock discontinuities: From classical to non-classical shocks. *Acta Mechanica*, *229*(2), 515–533. https://doi.org/10.1007/s00707-017-1984-3
Korup, O. (2008). Rock type leaves topographic signature in landslide-dominated mountain ranges. *Geophysical Research Letters*, *35*(11), L11402. https://doi.org/10.1029/2008gl034157
Lambare, G., Operto, S., Podvin, P., & Thierry, P. (2003). 3d ray+ born migration/inversion—Part 1: Theory. *Geophysics*, *68*(4), 1348–1356. https://doi.org/10.1190/1.1598128
Larsen, I. J., & Montgomery, D. R. (2012). Landslide erosion coupled to tectonics and river incision. *Nature Geoscience*, *5*(7), 468–473. https://doi.org/10.1038/ngeo1479
Lawton, D. C. (1989). Computation of refraction static corrections using first-break traveltime differences. *Geophysics*, *54*(10), 1289–1296. https://doi.org/10.1190/1.1442588
Lorenzo-Trueba, J., & Voller, V. (2010). Analytical and numerical solution of a generalized stefan problem exhibiting two moving boundaries with application to ocean delta formation. *Journal of Mathematical Analysis and Applications*, *366*(2), 538–549. https://doi.org/10.1016/j.jmaa.2010.01.008
Lorenzo-Trueba, J., Voller, V. R., Paola, C., Twilley, R. R., & Bevington, A. E. (2012). Exploring the role of organic matter accumulation on delta evolution. *Journal of Geophysical Research*, *117*(F4), F00A02. https://doi.org/10.1029/2012jf002339
Luke, J. C. (1972). Mathematical models for landform evolution. *Journal of Geophysical Research*, *77*(14), 2460–2464. https://doi.org/10.1029/jb077i014p02460
Luke, J. C. (1974). Special solutions for nonlinear erosion problems. *Journal of Geophysical Research*, *79*(26), 4035–4040. https://doi.org/10.1029/jb079i026p04035
Masoliver, J., & Ros, A. (2009). From classical to quantum mechanics through optics. *European Journal of Physics*, *31*(1), 171–192. https://doi.org/10.1088/0143-0807/31/1/016
Montgomery, D. R. (2001). Slope distributions, threshold hillslopes, and steady-state topography. *American Journal of Science*, *301*(4–5), 432–454. https://doi.org/10.2475/ajs.301.4-5.432
Montgomery, D. R., & Brandon, M. T. (2002). Topographic controls on erosion rates in tectonically active mountain ranges. *Earth and Planetary Science Letters*, *201*(3–4), 481–489. https://doi.org/10.1016/s0012-821x(02)00725-2
Montgomery, D. R., & Dietrich, W. E. (1994). A physically based model for the topographic control on shallow landsliding. *Water Resources Research*, *30*(4), 1153–1171. https://doi.org/10.1029/93wr02979
Montgomery, D. R., & Foufoula-Georgiou, E. (1993). Channel network source representation using digital elevation models. *Water Resources Research*, *29*(12), 3925–3934. https://doi.org/10.1029/93wr02463
Nadai, A. (1954). *Theory of flow and fracture of solids, 1950*. Google Scholar.
Nechaev, S., & Polovnikov, K. (2017). From geometric optics to plants: The eikonal equation for buckling. *Soft Matter*, *13*(7), 1420–1429. https://doi.org/10.1039/c6sm02438f
Oguchi, T., & Oguchi, C. T. (2010). *Mt. Fuji: The beauty of a symmetric stratovolcano* (pp. 303–309). Geomorphological Landscapes of the World.
Ohmori, H. (1993). Changes in the hypsometric curve through mountain building resulting from concurrent tectonics and denudation. *Geomorphology*, *8*(4), 263–277. https://doi.org/10.1016/0169-555x(93)90023-u
Ortiz, M., & Gioia, G. (1994). The morphology and folding patterns of buckling-driven thin-film blisters. *Journal of the Mechanics and Physics of Solids*, *42*(3), 531–559. https://doi.org/10.1016/0022-5096(94)90030-2

Ouimet, W. B., Whipple, K. X., & Granger, D. E. (2009). Beyond threshold hillslopes: Channel adjustment to base-level fall in tectonically active mountain ranges. *Geology*, *37*(7), 579–582. https://doi.org/10.1130/g30013a.1

Pauli, N. S., & Gioia, G. (2007). The topography of steady sandpiles on arbitrary domains. *Proceedings of the Royal Society A: Mathematical, Physical and Engineering Sciences*, *463*(2081), 1247–1258. https://doi.org/10.1098/rspa.2007.1812

Penck, W. (1953). Morphological analysis of land forms: A contribution to physical geology.

Perron, J. T., Kirchner, J. W., & Dietrich, W. E. (2009). Formation of evenly spaced ridges and valleys. *Nature*, *460*(7254), 502–505. https://doi.org/10.1038/nature08174

Petres, C., Pailhas, Y., Patron, P., Petillot, Y., Evans, J., & Lane, D. (2007). Path planning for autonomous underwater vehicles. *IEEE Transactions on Robotics*, *23*(2), 331–341. https://doi.org/10.1109/tro.2007.895057

Porporato, A. (2022). Hydrology without dimensions. *Hydrology and Earth System Sciences*, *26*(2), 355–374. https://doi.org/10.5194/hess-26-355-2022

Qi, Y., & Wang, M. (2001). The self-similar profiles of generalized kpz equation. *Pacific Journal of Mathematics*, *201*(1), 223–240. https://doi.org/10.2140/pjm.2001.201.223

Rodriguez-Iturbe, I., & Rinaldo, A. (2001). *Fractal river basins: Chance and self-organization*. Cambridge University Press.

Roering, J. J., Kirchner, J. W., & Dietrich, W. E. (1999). Evidence for nonlinear, diffusive sediment transport on hillslopes and implications for landscape morphology. *Water Resources Research*, *35*(3), 853–870. https://doi.org/10.1029/1998wr900090

Roering, J. J., Perron, J. T., & Kirchner, J. W. (2007). Functional relationships between denudation and hillslope form and relief. *Earth and Planetary Science Letters*, *264*(1–2), 245–258. https://doi.org/10.1016/j.epsl.2007.09.035

Royden, L., & Taylor Perron, J. (2013). Solutions of the stream power equation and application to the evolution of river longitudinal profiles. *Journal of Geophysical Research: Earth Surface*, *118*(2), 497–518. https://doi.org/10.1002/jgrf.20031

Rukhadze, A. A., & Silin, V. P. (1964). Method of geometrical optics in the electrodynamics of an inhomogeneous plasma. *Soviet Physics - Uspekhi*, *7*(2), 209–229. https://doi.org/10.1070/pu1964v007n02abeh003662

Sethian, J. A., & Adalsteinsson, D. (1997). An overview of level set methods for etching, deposition, and lithography development. *IEEE Transactions on Semiconductor Manufacturing*, *10*(1), 167–184. https://doi.org/10.1109/66.554505

Seybold, H., Berghuijs, W. R., Prancevic, J. P., & Kirchner, J. W. (2021). Global dominance of tectonics over climate in shaping river longitudinal profiles. *Nature Geoscience*, *14*(7), 503–507. https://doi.org/10.1038/s41561-021-00720-5

Singh, A., Reinhardt, L., & Foufoula-Georgiou, E. (2015). Landscape reorganization under changing climatic forcing: Results from an experimental landscape. *Water Resources Research*, *51*(6), 4320–4337. https://doi.org/10.1002/2015wr017161

Spacesystems, N., & Team, U. A. S. (2019). Aster global digital elevation model v003 [Dataset]. NASA EOSDIS Land Processes DAAC. https://doi.org/10.5067/ASTER/ASTGTM.003

Stark, C. P., & Stark, G. J. (2022). The direction of landscape erosion. *Earth Surface Dynamics*, *10*(3), 383–419. https://doi.org/10.5194/esurf-10-383-2022

Stock, J., & Dietrich, W. E. (2003). Valley incision by debris flows: Evidence of a topographic signature. *Water Resources Research*, *39*(4), 1089. https://doi.org/10.1029/2001wr001057

Strahler, A. N. (1950). Equilibrium theory of erosional slopes approached by frequency distribution analysis. Part I. *American Journal of Science*, *248*(10), 673–696. https://doi.org/10.2475/ajs.248.10.673

Strahler, A. N. (1952). Hypsometric (area-altitude) analysis of erosional topography. *Geological Society of America Bulletin*, *63*(11), 1117–1142. https://doi.org/10.1130/0016-7606(1952)63[1117:haaoet]2.0.co;2

Swenson, J., Voller, V., Paola, C., Parker, G., & Marr, J. (2000). Fluvio-deltaic sedimentation: A generalized stefan problem. *European Journal of Applied Mathematics*, *11*(5), 433–452. https://doi.org/10.1017/s0956792500004198

Tarboton, D. G., Bras, R. L., & Rodriguez-Iturbe, I. (1991). On the extraction of channel networks from digital elevation data. *Hydrological Processes*, *5*(1), 81–100. https://doi.org/10.1002/hyp.3360050107

Tucker, G., & Whipple, K. (2002). Topographic outcomes predicted by stream erosion models: Sensitivity analysis and intermodel comparison. *Journal of Geophysical Research*, *107*(B9), ETG–1. https://doi.org/10.1029/2001jb000162

Tucker, G. E., & Bras, R. L. (1998). Hillslope processes, drainage density, and landscape morphology. *Water Resources Research*, *34*(10), 2751–2764. https://doi.org/10.1029/98wr01474

Tucker, G. E., & Slingerland, R. L. (1994). Erosional dynamics, flexural isostasy, and long-lived escarpments: A numerical modeling study. *Journal of Geophysical Research*, *99*(B6), 12229–12243. https://doi.org/10.1029/94jb00320

Vardinoyannis, K., Tzatzi, M., & Mylonas, M. (2015). Terrestrial snails (Mollusca: Gastropoda) of the Gyaros island (Cyclades, Greece). *Folia Malacologica*, *23*(1), 41–46. https://doi.org/10.12657/folmal.023.005

Weissel, J. K., & Seidl, M. A. (1998). Inland propagation of erosional escarpments and river profile evolution across the southeast Australian passive continental margin. *Geophysical Monograph-American Geophysical Union*, *107*, 189–206.

Whipple, K. X., Kirby, E., & Brocklehurst, S. H. (1999). Geomorphic limits to climate-induced increases in topographic relief. *Nature*, *401*(6748), 39–43. https://doi.org/10.1038/43375

Whitham, G. B. (2011). *Linear and nonlinear waves*. John Wiley & Sons.

Zondervan, J. R., Stokes, M., Boulton, S. J., Telfer, M. W., & Mather, A. E. (2020). Rock strength and structural controls on fluvial erodibility: Implications for drainage divide mobility in a collisional mountain belt. *Earth and Planetary Science Letters*, *538*, 116221. https://doi.org/10.1016/j.epsl.2020.116221